
جامعة الملك عبدالله
للعلوم والتقنية
King Abdullah University of
Science and Technology

Improved Amott Cell Procedure for Predictive Modeling of Oil Recovery Dynamics from Mixed-Wet Carbonates

Item Type	Conference Paper
Authors	Kaprielova, Ksenia; Yutkin, Maxim; Gmira, Ahmed; Ayirala, Subhash; Radke, Clayton; Patzek, Tadeusz
Citation	Kaprielova, K., Yutkin, M., Gmira, A., Ayirala, S., Radke, C., & Patzek, T. W. (2022). Improved Amott Cell Procedure for Predictive Modeling of Oil Recovery Dynamics from Mixed-Wet Carbonates. Day 1 Mon, April 25, 2022. https://doi.org/10.2118/209444-ms
Eprint version	Post-print
DOI	10.2118/209444-ms
Publisher	SPE
Rights	Archived with thanks to SPE
Download date	27/09/2023 11:03:38
Link to Item	http://hdl.handle.net/10754/676519

SPE-209444-MS

Improved Amott Cell Procedure for Predictive Modeling of Oil Recovery Dynamics from Mixed-Wet Carbonates

Ksenia Kaprielova and Maxim Yutkin, King Abdullah University of Science and Technology; Ahmed Gmira and Subhash Ayirala, Saudi Aramco; Clayton Radke, University of California, Berkeley; Tadeusz W. Patzek, King Abdullah University of Science and Technology

Copyright 2021, Society of Petroleum Engineers

This paper was prepared for presentation at 23rd SPE Improved Oil Recovery Conference held online, April 25 – 29, 2022.

This paper was selected for presentation by an SPE program committee following review of information contained in an abstract submitted by the author(s). Contents of the paper have not been reviewed by the Society of Petroleum Engineers and are subject to correction by the author(s). The material does not necessarily reflect any position of the Society of Petroleum Engineers, its officers, or members. Electronic reproduction, distribution, or storage of any part of this paper without the written consent of the Society of Petroleum Engineers is prohibited. Permission to reproduce in print is restricted to an abstract of not more than 300 words; illustrations may not be copied. The abstract must contain conspicuous acknowledgment of SPE copyright.

Abstract

Spontaneous counter-current imbibition in Amott cell experiments is a convenient laboratory method of studying oil recovery from oil-saturated rock samples in secondary or tertiary oil recovery by waterflood of adjustable composition. Classical Amott cell experiment estimates ultimate oil recovery. It is not designed, however, for studying the dynamics of oil recovery. In this work we identify a flaw in the classical Amott cell imbibition experiments that hinders the development of predictive recovery models for mixed-wet carbonates. We revise the standard Amott procedure in order to produce smoother experimental production curves, which then can be described by a mathematical model more accurately. We apply Generalized Extreme Value distribution to model the cumulative oil production. We start with the Amott imbibition experiments and scaling analysis for Indiana limestone core plugs saturated with mineral oil. The knowledge gained from this study will allow us to develop a predictive model of water-oil displacement for reservoir carbonate rock and crude oil recovery systems.

Introduction

Carbonate reservoirs hold more than half of crude oil after primary and secondary production. Among different improved oil recovery techniques (IOR), low/modified salinity waterflooding (LSW) has attracted the oil industry's attention owing to its economic and environmental benefits. The method involves injection of brines with customized salinity and composition to improve mobility of crude oil in mixed-wet carbonates and thus increment oil recovery.

Rock wettability is one of the main characteristics that control crude oil recovery from mixed-wet carbonates by LSW (Moore and Slobod, 1955). It has been shown recently by experiment that slightly shifting rock wettability towards more water-wet results in spontaneous imbibition of brine into mixed-wet pores and thus may increment the oil recovery (Saad et al., 2022). The mechanism of crude oil detachment, however, is still under debate due to complex interactions in crude oil/brine and brine/carbonate rock interfaces (Brady and Thyne, 2016; Yutkin et al., 2021, 2022). Despite these uncertainties, many research groups have reported a notable increase in crude oil recovery by treating the oil-saturated carbonate samples with modified salinity brines (Zhang et al., 2006; Fathi et al., 2010; Ayirala et al., 2020). Laboratory findings, however, are rarely implemented at reservoir scale. Very few studies reported field pilot results on LSW (Yousef et al., 2012).

Spontaneous imbibition in Amott cells is a commonly used laboratory technique to explore the effect of LSW brine composition on oil recovery from oil-saturated rock samples. An Amott cell is a glass jar with a small-diameter graduated-glass-burette attached to the top to measure history of volumetric oil production. An oil-saturated core plug is placed into the Amott cell and the tested brine is poured into the jar. Brine being the wetting phase imbibes into the rock and displaces the non-wetting oil phase. Counter-current spontaneous imbibition of brine into an oil-saturated rock core plug is governed by capillary pressure and wettability, and therefore it may represent at centimeter scale oil displacement in a reservoir during secondary or tertiary recovery by low/modified-salinity waterflooding.

Originally, Amott cells were used to evaluate ultimate oil recovery during spontaneous imbibition of brine and oil into the rock samples saturated with oil and brine, respectively (Amott, 1959). The wettability indices were then defined as the ratios of the spontaneous displacement volumes to the total displacement volumes. In later studies, rock wettability state was inferred from the dynamics of oil recovery in Amott cell experiments (Morrow et al., 1999; Morrow and Mason, 2001; Kashchiev and Firoozabadi, 2002). The studies have reported that for mixed-wet pores the recovery dynamics depends heavily on the pore wettability state that is defined by complex interactions at the crude oil/brine and brine/carbonate rock interfaces. However, it is rarely mentioned that during spontaneous imbibition into mixed-wet rock samples, the released oil ganglia adhere to the mixed-wet or oil-wet outer rock surface in the form of sticky oil droplets (Graue et al., 1999; Morrow et al., 1999; Babadagli, 2002; Clerke et al., 2013; Cobos et al., 2021). These droplets grow large before buoyancy detaches them, and thus oil production profile becomes jagged and masks recovery dynamics. To minimize

this effect, the oil droplets were removed from the core surface before every measurement by either shaking the Amott cell (Graue et al., 1999; Cobos et al., 2021), or with the aid of a teflon rod (Morrow et al., 1999; Zhou et al., 2000).

Some authors modified spontaneous imbibition experiments to improve accuracy of data recording. For example, Zhou et al. (2000) and Ghedan et al. (2009) suspended a rock sample in brine *via* a thin rope connected to a balance that recorded the change in the core weight. The oil displacement profile was then determined gravimetrically. In another example, the quasi-spontaneous imbibition of brine was conducted in a centrifuge at a low speed of 190 rpm, and oil production was monitored volumetrically with a high resolution camera (Clerke et al., 2013). Centrifuge cups block production from core sides and leave only the top disk face to imbibe and produce from, which greatly slows the process. In addition, estimates of oil droplet volumes from time-lapse images are prone to a large error that might cause cumulative oil production to decrease with time (see Fig. 13 in (Clerke et al., 2013)). All the described modifications of Amott's experimental procedures did not eventually ensure a smooth profile of the recovered oil, nor did they allow for temperature control.

We believe that the crude-oil-holdup artifacts hinder the development of predictive recovery models for mixed-wet carbonates. In this work, we suggest modifications to the classic Amott cell experimental procedure and explore their effects on oil production dynamics. We use orbital shaking to detach oil droplets from the outer rock surface. In addition, we mask top and bottom core faces to enforce 1D radial, two-phase flow. The proposed modifications do not require sophisticated equipment and can be implemented in a laboratory oven at moderate temperatures. These modifications result in the smoother oil recovery curves from both water-wet and mixed-wet limestone core samples. We hope that the production rates and final recoveries obtained with the revised approach can be described with a spontaneous imbibition model more accurately.

Classical continuum models of spontaneous imbibition in oil-water systems, that can be traced back to Richards (1928, 1931), Muskat (1937) and Rapoport and Leas (1953), are inadequate. These models represent transport in an essentially transient nonequilibrium process with *equilibrium* capillary pressure curves and *steady state* relative permeabilities. With time, this mix of inconsistent choices was termed "equilibrium" model of spontaneous imbibition. Such terminology is faulty at best and should not be used. "Classical models of spontaneous imbibition," or "Richards' approach" might be used instead. The Barenblatt et al.'s imbibition model, Barenblatt (1971); Barenblatt and Vinnichenko (1980); Barenblatt and Gilman (1987); Barenblatt et al. (2003), aims to correct the deficiencies of the classical models of spontaneous imbibition, but it cannot be applied to all cases of spontaneous imbibition without (1) checking its applicability and (2) investigating relaxation time(s) of oil/water interfaces.

Silin and Patzek (2004) have developed the scaling of countercurrent spontaneous imbibition experiments into a large block of homogeneous isotropic rock with no initial water saturation. Spontaneous imbibition with initial water is a very different process than spontaneous imbibition without initial water. The difference is enough to justify *completely different treatments*. In natural water-wet systems, the matrix blocks are initially filled with oil and water, and the natural fractures are initially filled with oil and (perhaps) gas, but with very little water. The injected/surrounding water must displace the oil and gas from the fractures for the countercurrent imbibition to proceed. "Connate water" in a *water-wet* rock remains connected throughout the rock. The connate water saturation is set by the highest capillary pressure during primary drainage in which oil accumulated in the rock. Thus the water is not only connected, but ready to flow, and could be squeezed out from the rock if capillary pressure were increased further. Only a small part of the connate water is chemically bound in the pore-wall lining clays and other minerals. This observation pertains to most sandstones, carbonates (including chalks and microporous muds), and the silicious mudrock diatomites Zhou et al. (2001).

As a first step in charting our new approach to modeling countercurrent imbibition in the presence of connate water, we apply Generalized Extreme Value (GEV) statistics (Gumbel, 1958) to model cumulative oil recovery.

Modified Amott Cell

Originally, the Amott cell was not designed to study the dynamics of oil recovery/imbibition. Some oil (be it refined oil or crude oil) produced during spontaneous counter-current imbibition is trapped by capillary forces at the rock sample surface. That is, oil droplets remain on the rock sample surface until they grow sufficiently large by coalescence or production. Such behavior obscures production dynamics. **Figure 1** exemplifies this effect in a typical Amott imbibition experiment. That Amott cell was not disturbed during the experiment. Note the long periods of zero production rate (constant cumulative recovery) and abrupt jumps when a few large drops detach from the surface when buoyancy overcomes interfacial tension forces. This effect is more pronounced in the case of oil-wet or mixed-wet rock, and in the presence of gas. The result is random hiccups in cumulative oil recovery during the imbibition process. Only a handful of authors mention these problems and the ways they dealt with them (Graue et al., 1999; Morrow et al., 1999; Babadagli, 2002; Clerke et al., 2013; Cobos et al., 2021).

Another issue that hinders interpretation of production dynamics is flow geometry during an experiment. In a typical Amott imbibition experiment, brine imbibes from all sides. However, the imbibition rates for top and bottom faces are different and so is the axial imbibition rate. In contrast to the aforementioned oil droplet adhesion, this issue is discussed more frequently and thoroughly in the literature (Kashchiev and Firoozabadi, 2002; Babadagli, 2002; Ghedan et al., 2009).

In an attempt to address these serious issues and be able to observe more realistic dynamics of imbibition, we introduce several changes to the Amott-cell design and experiment execution.

First, we cover the top and the bottom faces of core plugs to block completely their contributions to production. After testing several

cover designs, we settled on using solid glass discs. The 6.5-mm thick discs were fabricated from borosilicate glass. **Figure 2** shows a way to fix these discs to the core plug with the least possible loss of the outer surface. The glass disc is of the same diameter as the core plug (Fig. 2a). Then a narrow band of heat-shrinkable Viton sleeve is fitted onto the glass disc and part of the core, and fixed by gentle heating with a heat gun (Fig. 2b). Next, we place a heat-shrinkable thin teflon sleeve on top of the Viton sleeve (Fig. 2c) and again fix it with gentle heating. Both Viton and teflon sleeves shrink upon heating and firmly fix the glass discs in place (Fig. 2d). The materials for glass discs fixation were carefully selected; the Viton sleeve has some flexibility and therefore provides a good seal for a core sample placing in the cell. The teflon sleeve is omniphobic and prevents oil accumulation on it. This design is easy, cheap, and fast in implementing. The tight fitting of the discs *via* a heat-shrinkable sleeve prevents accumulation of the oil droplets on the top and bottom sample surfaces.

Next, to dislodge oil droplets from the now only available cylindrical rock surface, we introduce a continuous circular motion of the Amott cell using an orbital shaker shown in **Figure 3**. The shaker continuously rotates the Amott cells with a small orbit (19 mm) during the entire testing period with regular short stops for oil-production measurement. To immobilize a core plug during the Amott cell motion, the plug is lowered into a custom-made glass seat at the bottom of the cell shown in **Figure 4**. The narrow band of the heat-shrinkable sleeve fastened at the sample bottom fixes snugly the core plug in the seat. The above modifications require that the Amott cell be manufactured from two glass flanges joined with a clamp in the middle of the main cell body (Fig. 4a and 4b). This design ensures the convenient placement of a core plug in the glass seat. Fig. 4c demonstrates the assembled Amott cell with the core sample fixed in the glass seat and filled with a brine solution.

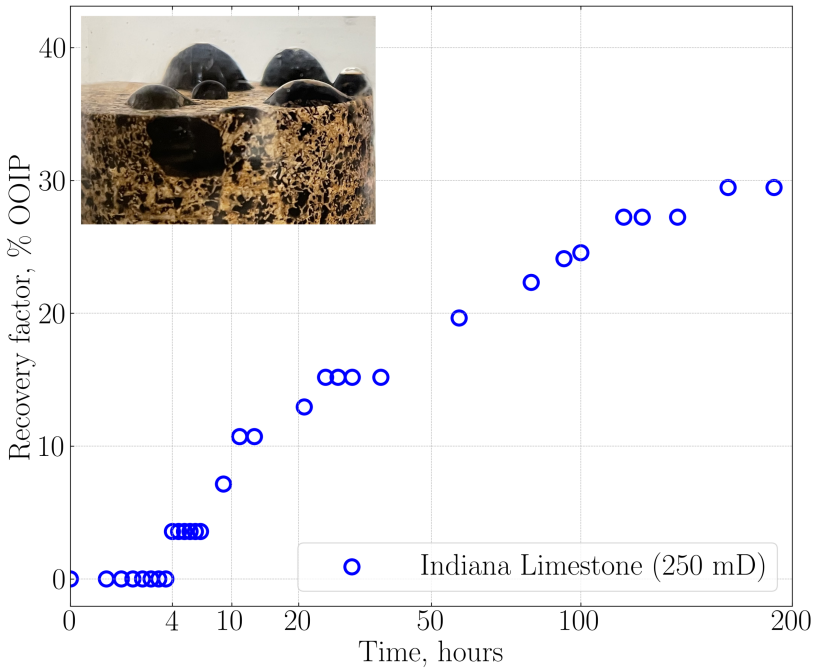

Figure 1: Cumulative crude oil recovery versus square root of time in a typical Amott cell spontaneous imbibition experiment. The top left picture demonstrates the adhesion of crude oil droplets to the core-plug top external surface during the imbibition experiment. These oil droplets grow large and detach from the rock surface causing stepwise profile of oil recovery.

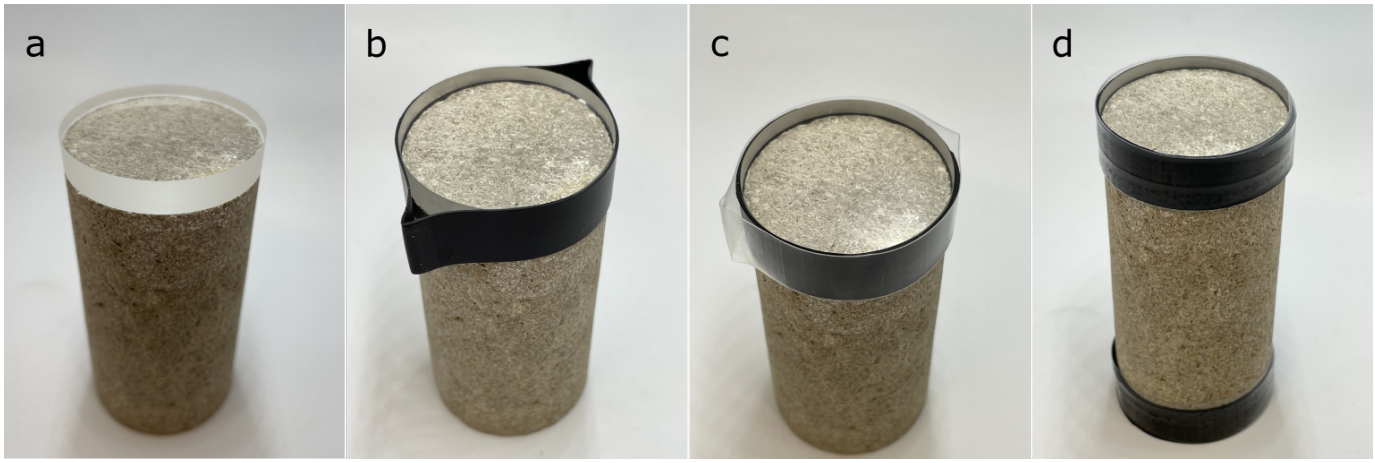

Figure 2: The core plug preparation for Amott cell imbibition experiment: a) glass discs are used to cover the base of a core plug; b) a band from Viton sleeve is used to fix the glass discs, the band shrinks with heating by a heat gun; c) a band made from teflon sleeve is fixed above by the heat gun; d) both top and bottom bases are covered.

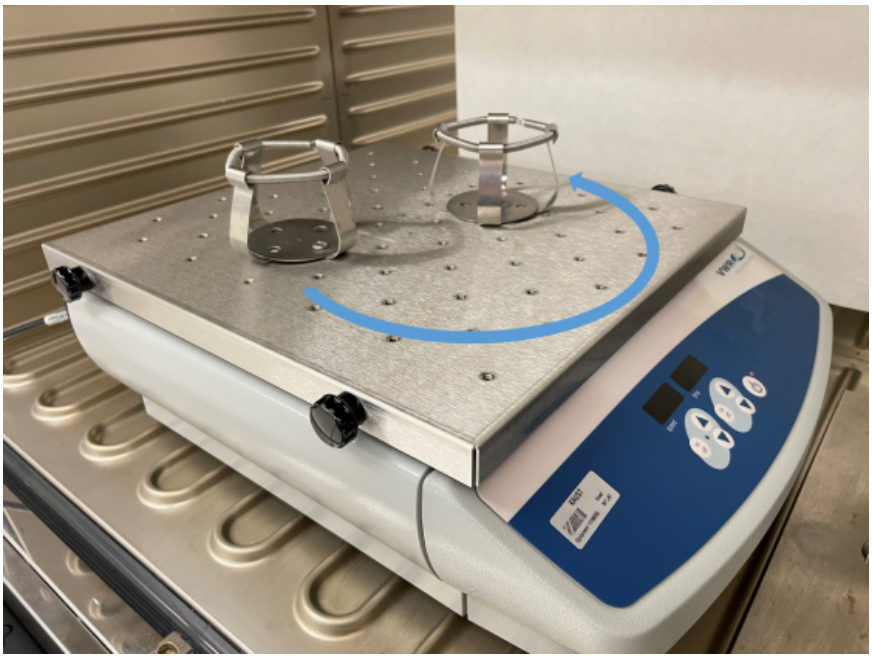

Figure 3: VWR Advanced orbital shaker used for Amott cell shaking during the spontaneous imbibition experiments. The rotation speed is 200 RPM and the rotor orbit is 19 mm.

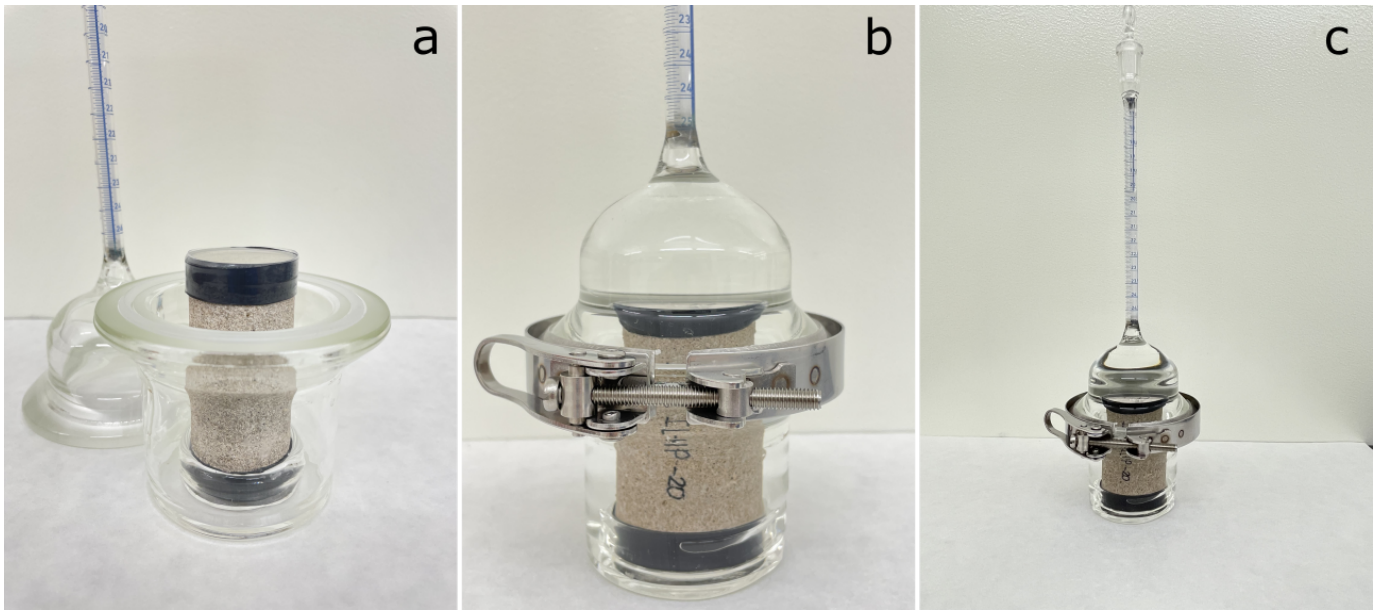

Figure 4: The modified Amott cell: a) a core plug sample is fixed in the glass seat at the bottom of the cell to preserve lateral stability of the sample during shaking; b) the top and the bottom flanges of the Amott cell are fastened with a clamp; and c) the assembled Amott cell with a sample and a brine solution.

Methodology

Core Samples and Solutions. Indiana Limestone core plugs 1.5 in. by 12 in. were received from Kocurek Industries, Inc., and cut into 3 in. length samples that were used in all experiments. The gas porosity was measured using a PDP-300 Helium Boyle's law porosimeter (MetaRock Laboratories). The core plug porosity and permeability were measured with 0.1M NaCl using the CFSH2B Basic Core Flood System (MetaRock Laboratories). The measurements were performed at the confining pressure of 500 psi, back-pressure of 150 psi, and at Reynolds numbers less than 1.

Brine solutions for core-plug saturation and for imbibition experiments were prepared from chemicals received from Fisher Scientific (ACS or reagent grade). Water was purified with Milli-Q Advantage A10 system (Millipore). Mineral oil solutions for core samples saturation were received from Fisher Scientific. Mineral oil light (O121-4, Lot 096089) was diluted with hexadecane (mineral oil light 85 wt.% , hexadecane 15 wt.%) and referred to as Oil-1. Mineral oil heavy (O122-4, Lot 094087) was used as received and referred to as Oil-2. Viscosities of the used mineral oil solutions were measured using Anton Paar MCR 302 rheometer with the CC27 measuring system.

Core Plug Saturation with Mineral Oil. The brine-filled core plugs were saturated with mineral oil using the ANPERC's 10-Cell System (MetaRock Laboratories). A core sample saturated with 0.1M NaCl brine was placed in the Hassler-type core holder with a rubber sleeve and confined to 500 psi. The mineral oil was injected at ambient temperature and the constant pressure of 80 psi using ISCO Pump (260D, Teledyne ISCO). In the case of viscous mineral oil (Oil-2), the core plugs were saturated at 60 °C. Hydrophilic ceramic porous plate (the breakthrough pressure of 217 psi) was placed at the bottom of the core plug to allow a homogeneous distribution of mineral oil within the porous rock. To estimate average oil saturation, the displaced brine was collected in the calibrated burette at the outlet of the core holder. Typically, saturation with mineral oil was conducted over one or two days, until 70-80% of oil saturation was reached.

Spontaneous Imbibition in Amott Cell. After a core sample was saturated with oil, the top and the bottom of the sample were covered with the glass discs and fastened with the heat shrinkable band (Fig. 2), then fixed in the glass seat of the Amott cell (Fig. 4). The flooding brine (0.1 M NaCl) was poured into the Amott cell to the top of the graduated burette. It is important to preheat and degas the brine to avoid formation of small gas bubbles at the core sample surface.

The VWR Advanced orbital shaker model 3500 (Henry Troemner LLC) was used in the experiments. This model can operate at high humidity and elevated temperatures. Up to two Amott cells with the samples and brines were mounted on the shaker that was placed in the oven (**Figure 5**). The experiments were conducted at 60°C. The Amott cells were continuously shaken at 200 RPM (orbit 19 mm) during the experiments with short stops for oil production measurement. The expelled volume of oil was measured as a function of time. Usually a pair of samples with close characteristics were tested at shaking and at static (no disturbance of the Amott cell during the whole testing period) conditions for comparison (Fig. 5). For static testing, the core samples were prepared similarly, and the top and bottom sides were covered with the glass discs to have a similar surface geometry for imbibition.

Figure 5: Two pairs of core plugs in the modified Amott cells are tested at constant shaking (left cells mounted on the shaker platform), and at static conditions (right cells).

Spontaneous Imbibition Results

We have tested five pairs of core-plug samples with the similar petrophysical characteristics at shaking and static conditions to estimate the effect of the Amott cell motion. The characteristics of the core plugs and the experimental parameters of the Amott-cell testing are summarized in **Table 1**.

Figure 6 compares the results of spontaneous imbibition for IL-6 and IL-7 core plugs at constant shaking and at static conditions, respectively, on a square root of time scale. These core plugs were cut from the same 12 inch-long core and therefore have close petrophysical properties (Fig. 6). For both core plugs, the recovery rate was rather fast, oil production started almost immediately, and similar ultimate recovery was quickly reached within the first 24 hours. The square root of time production dependence is notable during the first several hours of the production. The difference between the static and the shaking experiments is small, but easily observable between 4 and 16 hours of imbibition. For the static test in about 3 hours of oil production the Amott cell was rotated to make a photo that helped the oil droplets to detach from the core surface and artificially changed the recovery profile (Fig. 6).

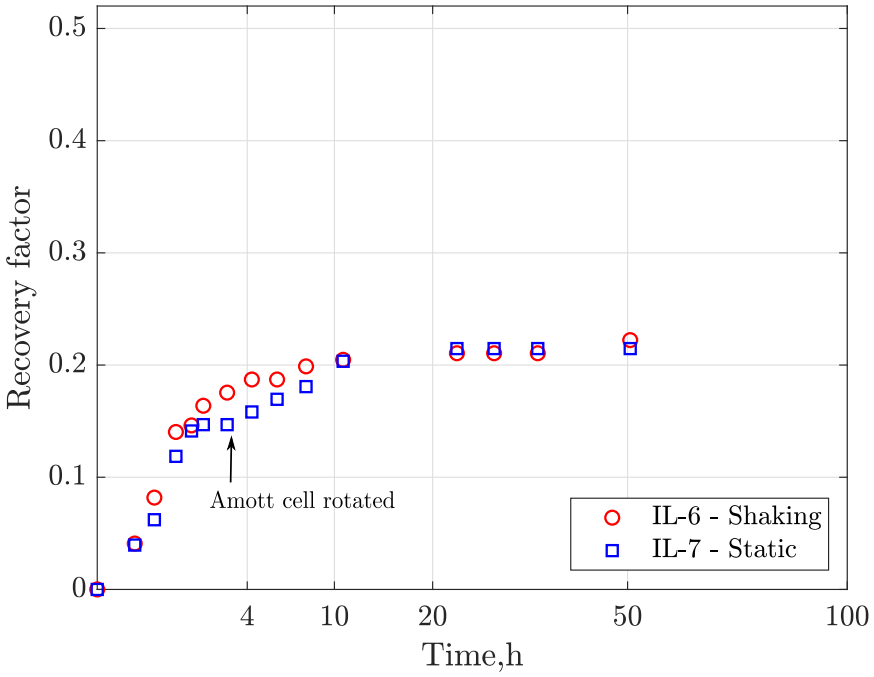

Figure 6: Experimental cumulative recovery (fraction OOIP) versus square root of time. Core IL-6, shaking, $k = 19$ **md,** $\phi = 0.148$**,** $\mu_o = 7.3$ **cp; core IL-7, static,** $k = 41$ **md,** $\phi = 0.151$**,** $\mu_o = 7.3$ **cp.**

After the spontaneous imbibition experiments from Fig. 6 samples IL-6 and IL-7 were resaturated with the same Oil-1 and again tested in spontaneous imbibition. **Figure 7** shows the recovery profiles for resaturated core plugs referred to as IL-6a and IL-7a. Here the difference in the production between the shaking and static experiment is more pronounced. For the static test the oil production goes in a stepwise fashion, while the shaking tests gives a smooth recovery curve. The oil ultimate recovery in Fig. 7 is slightly lower than that in Fig. 6, which we attribute to inaccurate estimation of the residual oil in the core plugs after the imbibition experiment (the

Table 1: Petrophysical characteristics of Indiana Limestone core plugs and experimental parameters of the Amott imbibition tests

Sample Code	φ (He), %	φ (Brine), %	κ (Brine), mD	Oil Code	Oil μ, cP (60°C)	Oil saturation (S_{oi}),%	Recovery, % OOIP	Imbibition regime
IL-6	16.6	14.8	19	Oil-1	7.3	69	22	shaking
IL-7	16.5	15.1	41	Oil-1	7.3	70	21	static
IL-6a	16.6	14.8	19	Oil-1	7.3	72	18	static
IL-7a	16.5	15.1	41	Oil-1	7.3	74	17	shaking
IL-6b	16.6	14.8	19	Oil-1	7.3	73	21	shaking
IL-7b	16.5	15.1	41	Oil-1	7.3	70	21	shaking
IL-20	17.0	16.0	37	Oil-1	7.3	73	22	shaking
IL-21	16.6	15.1	27	Oil-1	7.3	75	17	static
IL-22	17.0	15.5	38	Oil-2	23.5	81	14	static
IL-23	17.6	16.0	49	Oil-2	23.5	72	22	shaking

oil droplets stuck on the core surface were not counted). For shaking tests in Figs. 6 and 7 the core plugs demonstrate similar production profiles, as expected for the samples with similar characteristics.

Figure 8 shows a zoom-in view at the IL-6a outer core surface during the static imbibition experiment shown in Fig. 7. Note the large oil drops on the core surface. Because mineral oil does not change rock surface wettability, this is a capillarity-driven oil holdup effect. These drops can be detached with the slightest disturbance, but until that or buoyancy detachment they cling to the core surface and do not contribute to the production. The oil hold-up caused a pronounced stepwise profile of the oil recovery in Fig. 7. In the case of shaking the displaced oil easily detached from the rock surface and immediately contributed to the recovery profile. The experiments in both Fig. 6 and Fig. 7 clearly demonstrate that the modified Amott-cell imbibition procedure generates smoother recovery profiles, which is important for describing the production rates and recovery dynamics more precisely.

The introduced shaking motion of the Amott-cell does not remove all oil droplets from the outer core surface and thus does not fully eliminate the oil hold-up effect. Nevertheless, our approach significantly mitigates this effect in comparison with the static regime. We explore if such mitigation is sufficient to apply the scaling models below.

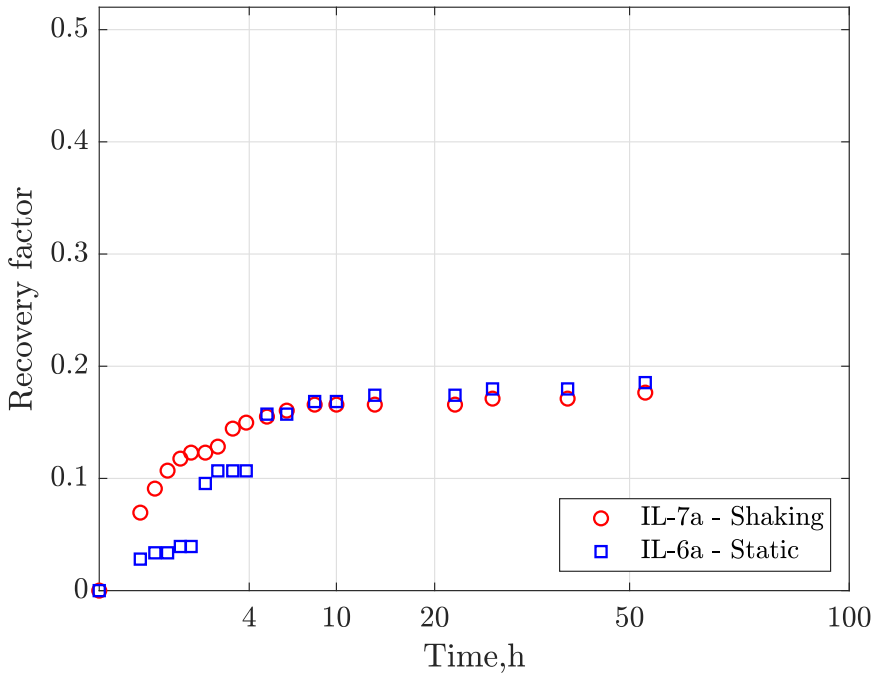

Figure 7: Experimental cumulative recovery (fraction OOIP) versus square root of time. Core IL-7a, shaking, $k = 41$ **md,** $\phi = 0.151$**,** $\mu_o = 7.3$ **cp; core IL-6a, static,** $k = 19$ **md,** $\phi = 0.148$**,** $\mu_o = 7.3$ **cp.**

To evaluate reproducibility of the results at shaking conditions samples IL-6a and IL-7a from Fig. 7 were properly cleaned, dried and resaturated again, first with a brine and then with the same Oil-1. **Figure 9** demonstrates the recovery profiles for cleaned and resaturated core plugs referred to as IL-6b and IL-7b, both in the shaking regime. For both IL-6b and IL-7b samples the oil recovery curves look smooth and completely reproduce the first shaking experiment (sample IL-6 in Fig. 6). These results confirm good reproducibility of the implemented Amott cell experiments.

To generate enough experimental data for scaling, we compare spontaneous imbibition against less viscous and more viscous mineral oils in the other two pairs of Indiana limestone core plugs. **Figure 10** shows the spontaneous imbibition results for samples IL-20 and IL-21, saturated with the less viscous Oil-1 with the viscosity of 7.3 cp. **Figure 11** demonstrates similar results for samples IL-22 and IL-23, saturated with the more viscous Oil-2 with the viscosity of 23.5 cp. These four new samples were cut from another 12 inch-long core, they also have similar petrophysical properties among themselves (see Table 1), but differ from samples IL-6 and IL-7.

Although samples IL-20 and IL-21 are similar to samples IL-6 and IL-7, and the same mineral oil (less viscous), the production rates are noticeably slower. In Fig. 10 the initial production is delayed and reaching the ultimate recovery takes a significantly longer time in comparison to that in Fig. 6 (note $\sim$1 hr offset), although the ultimate production in Fig. 10 is slightly higher. Because the IL-6/7 and IL-20/21 rock sample pairs have similar petrophysical properties and oil saturation (see Tables 1), we attribute production rate dissimilarities between them to the different pore structures and/or nonuniformity of oil saturation. By now, we cannot provide more evidence to support this claim, because we lack mercury intrusion data and X-Ray CT scan data.

Figure 10 shows the oil recovery profile for another pair of core plugs, IL-22 and IL-23. Because these samples were cut from the same core, and have nearly identical petrophysical properties and oil saturation, we expect them to behave similarly to samples IL-20 and IL-21. Except that samples IL-22 and IL-23 were saturated with the more viscous Oil-2 with 3 times higher viscosity than the oil

used in the experiments with samples IL-20 and IL-21. Therefore, we anticipate even slower overall production and initial production delay from IL-22 and IL-23. Indeed, initial production delay for IL-22 and IL-23 in Fig. 11 is longer by up to 2.5 hours. However, the overall production for IL-22 and IL-23 is not that different from those for IL-20 and IL-21, despite the 3-fold difference in oil viscosity.

In both Fig. 10 and Fig. 11 we observe a large difference between the static and dynamic experiments. Not only is the static production profile stepwise, but also oil production in static experiments is much slower than that in the dynamic experiments. Comparing the total recoveries for the IL-20/IL-21 pair at the end of the experiment, it would take IL-21 at least another 10+ hours to reach the ultimate production level of IL-20. As expected, the difference is more pronounced between IL-22 and IL-23 in Fig. 11 than between IL-20 and IL-21 in Fig. 10, because of the higher oil viscosity.

Finally, in all our spontaneous imbibition experiments with Indiana limestone core plugs and mineral oil, the ultimate recovery did

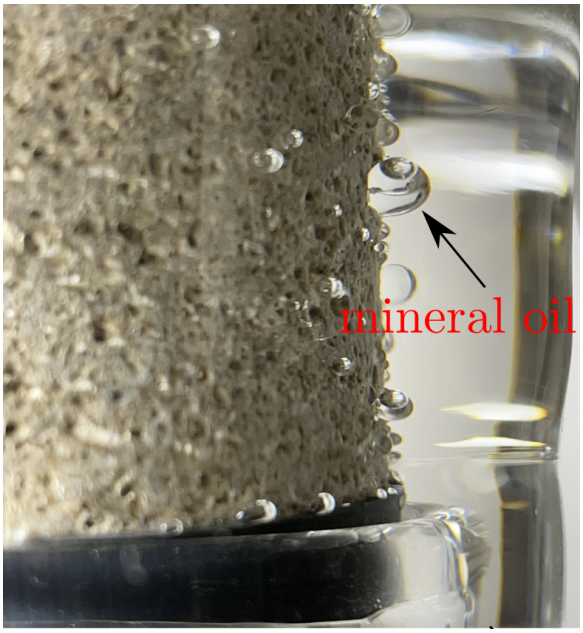

Figure 8: Mineral oil droplets displaced from the core plug during spontaneous imbibition are held onto the rock surface because of capillary-end effect.

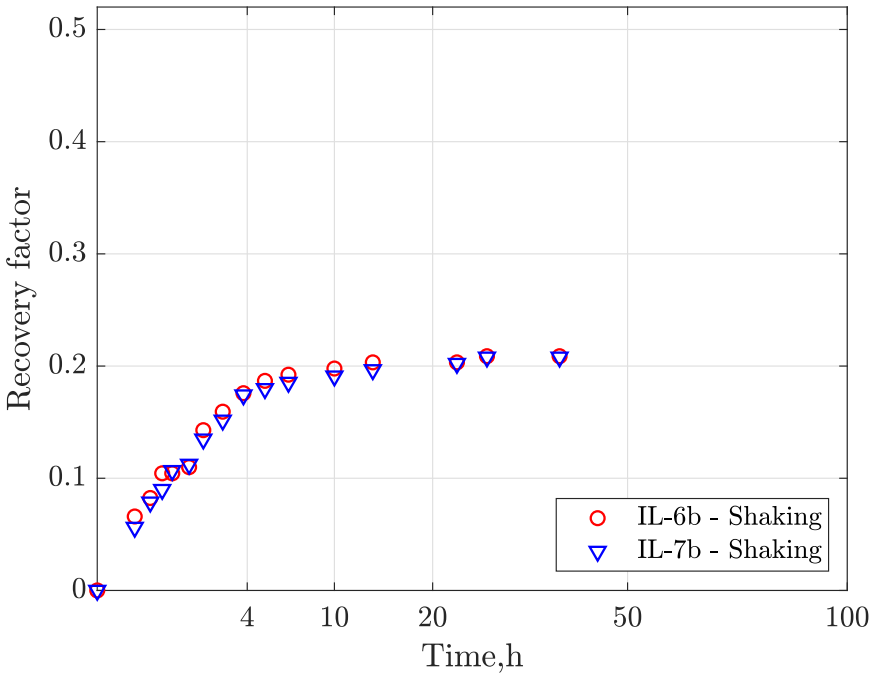

Figure 9: Experimental cumulative recovery (fraction OOIP) versus square root of time. Core IL-6b, shaking, $k = 19$ md, $\phi = 0.148$, $\mu_o = 7.3$ cp; core IL-7b, shaking, $k = 41$ md, $\phi = 0.151$, $\mu_o = 7.3$ cp.

not exceed 30% of OOIP. This is lower than those for chalk and sandstones (Tang and Firoozabadi, 2001; Graue et al., 1999). The reason for this outcome can be attributed to the complex multiscale pore structure of microporous limestones and the pronounced snap-off effect that dominates oil trapping in strongly water-wet pores of appropriate aspect ratios (Roof, 1970; Lenormand and Zarcone, 1989; Morrow et al., 1999; Liu et al., 2020).

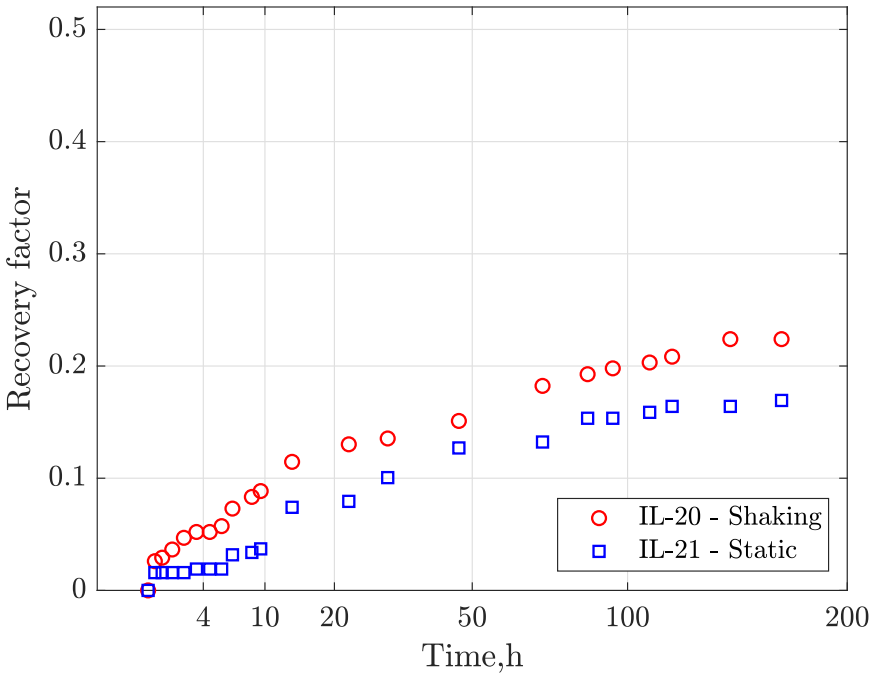

Figure 10: Experimental cumulative recovery (fraction OOIP) versus square root of time. Core IL-20, shaking, $k = 37$ **md,** $\phi = 0.160$**,** $\mu_o = 7.3$ **cp; core IL-21, static,** $k = 27$ **md,** $\phi = 0.151$**,** $\mu_o = 7.3$ **cp.**

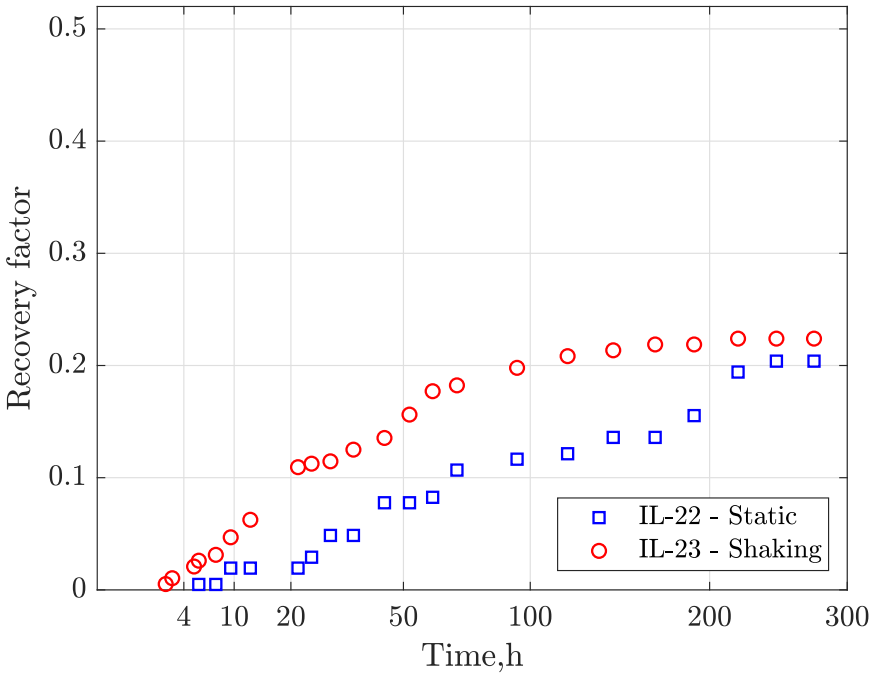

Figure 11: Experimental cumulative recovery (fraction OOIP) versus square root of time. Core IL-23, shaking, $k = 49$ **md,** $\phi = 0.160$**,** $\mu_o = 23.5$ **cp; core IL-22, static,** $k = 38$ **md,** $\phi = 0.155$**,** $\mu_o = 23.5$ **cp.**

Scaling of Spontaneous Imbibition

In this work we model spontaneous imbibition into a single block of permeable, strongly water-wet rock, here a cylindrical core that imbibes radially. The block is large enough, so that *early* imbibition from parts of the block surface can be treated as one-dimensional countercurrent imbibition into a semi-infinite porous medium. Early on, the cylinder circumference "feels" to the imbibing water like a plane. At intermediate and late times, the imbibition starts "feeling" water flow convergence towards the cylinder axis and other effects of water percolation.

The adjective "spontaneous" denotes a process that occurs because water inside the block is at a lower pressure than that than outside of it. Therefore a force exists that pulls the water into the block in a time-dependent flow. The essential reason for the water flow is lack of mechanical equilibrium. Thus, there is no such phenomenon as "equilibrium imbibition" and the adjective "nonequilibrium" is unnecessary when referring to spontaneous imbibition. The not-so-tacit assumption of the "non-equilibrium" description of fluid flow in spontaneous imbibition is that somehow in an "equilibrium" flow water would use the smallest channels and oil the largest, while in a "non-equilibrium" flow water would temporarily enter some of the largest channels, otherwise accessed only by oil. This whole argument would only be true if "equilibrium spontaneous imbibition" existed *and* if somehow the "non-equilibrium imbibition" were faster or slower than the equilibrium one.

The key factor controlling imbibition is the presence of water in the pore wall corners and roughness. The behavior of spontaneous imbibition *bifurcates* depending on the initial presence of water throughout the rock. So we consider two completely different non-equilibrium processes that occur in a water wet permeable rock with the initial water or without it.

Without the initial water, the imbibition process proceeds by a series of Concus-Finn capillary instabilities, which we have called the "corner filament collapses". The time scale of these instabilities is roughly constant, resulting in an almost constant delay time τ. Even more importantly, water imbibes as a diffuse "front" so the classical machinery that describes water imbibition can be used. This is the case solved by Silin and Patzek (2004) and illustrated with the corresponding experimental results. The experiments they used from Zhou et al. (2001), had no initial water in the rock.

With initial water saturation in the rock, the situation is diametrically different. Water flows in the corner filaments, snaps-off and either proceeds through a series of cooperative pore body-fillings to produce compact clusters growing throughout the rock, or not (Patzek, 2001). The ease of growing the water-invaded compact clusters depends on the pore aspect ratios. With the initial water one cannot speak of a diffuse "front" anymore. The process is essentially percolative and can be visualized as suburbs (water clusters) sprouting away from the downtown of a large city (the water inlet face). A different description of the imbibition process is required here (Lenormand, 1986, 1989, 1990).

The scaling theory developed by Silin and Patzek (2004) cannot be applied to our experiments without fundamental changes. This theory was developed for the water-free long cores, fully saturated with oil and imbibed along the axis. In our experiments, water flow is radial and has azimuthal dependence caused by rock inhomogeneities. What appears as pressure interference is a complex juxtaposition of several phenomena: (i) water penetration depth becomes large enough for the radial convergence of flow to reveal itself; (ii) the corner water menisci gradually swell everywhere in the core when capillary pressure decreases and squeeze some more oil out; and (iii) the invading water bypasses some oil, and causes cooperative pore body filling and snap-off (Patzek, 2001). The water filled clusters that emerge depend strongly on the rate of imbibition (wettability state) and pore body/pore throat geometry (Lenormand, 1989).

In this work, we apply Generalized Extreme Value (GEV) statistics to model cumulative oil recovery from Indiana limestone core plugs (IL-6 and 7, IL-6b and 7b, and IL-20 through 23). The details of the modeling are described below.

GEV Model. Generalized Extreme Value (GEV) statistics (Gumbel, 1958) models the distributions of minima or maxima of blocks of data. We apply GEV statistics to model cumulative oil recovery from the cores initially containing water. We posit that oil droplets exuded at the core circumference are the result of emptying many (hundreds) pores in a dynamic and somewhat cooperative manner. Therefore, each droplet's volume is a maximum of what the core surface could hold against surface tension and gravity, when the oil flows from a cluster of pores connected to the large pore where the droplet appears on the surface. The sizes and frequency of emergence of these droplets are given by an extreme value probability density function (pdf), whose scaled time integral is the cumulative recovery function RF.

In a generalized extreme value distribution of a random variable X that has outcomes x, $\mu \in \mathbb{R}$ is the *location parameter*, $\sigma > 0$ the *scale parameter*, and $\xi \in \mathbb{R}$ (often denoted by k) is the *shape parameter*. Always

$$1+\xi(x-\mu)/\sigma > 0 \tag{1}$$

The probability density function is

$$\begin{aligned} \mathrm{pdf}(x;\mu,\sigma,\xi) = &\frac{1}{\sigma}\left[1+\xi\left(\frac{x-\mu}{\sigma}\right)^{(-1/\xi)-1}\right]\times \\ &\times \exp\left\{-\left[1+\xi\left(\frac{x-\mu}{\sigma}\right)\right]^{-1/\xi}\right\} \end{aligned} \tag{2}$$

The cumulative distribution function (cdf) is an integral of Eq. (1). For example, when $\xi > 0$

$$\text{cdf}(x;\mu,\sigma,\xi) = \exp(-((x-\mu)/\sigma)^{-\xi}) \tag{3}$$

We scale experimental recovery factors, RF(t) (here time, t, replaces the random variable, x, in Eq. (3)), by the ultimate recovery (if known) RF_∞. We also set the pdf's location parameter $\mu = 0$ in all cases, and scale experimental time by the unknown average pressure diffusion time, τ (Patzek et al., 2013).

Scaling Results. Figures 12 – 15 summarize the scaling results for the pairs of samples IL-6/IL-7, IL-6b/IL-7b, IL-20/IL-21, and IL-22/IL-23, respectively. **Table 2** summarizes the GEV model fit parameters. Scaling results for each core pair contain two models: optimized scaling for each sample (*i.e.* the least square error, solid black line) and scaling based only on the endpoints of the recovery curve (dotted blue line).

We cannot explain yet the differences between the two pairs of experiments, IL-6/IL-7 and IL-20/IL-21. The latter two experiments have interference times that are an order (or two orders) of magnitude longer than the former ones. However, the duration of IL-6/IL-7 is almost four times shorter than that of L-20/IL-21.

In cores IL-22 and IL-23, a viscous 23.5 cp oil resulted in very slow recovery and persistence of the square root of time regime over the durations of both experiments. For the IL-22 experiment, σ is the slope and ξ the intercept of the square root of time line.

The key observation is that the cumulative recovery curve bends down below the square root of time trend when $t \geq 0.6\tau$ (Patzek et al., 2013). We thus assume that after the initial (during the first few minutes or hours of flow), vigorous rearrangement of water/oil interfaces, cumulative recovery grows for while as square root of time. Later, flow convergence and pressure interference dominate and the recovery curve bends down.

Table 2: Scaling results for the Amott spontaneous imbibition experiments

Name	Type	RF_∞	Oil μ, cp	τ, hr	μ	σ	ξ
IL-6	Shaking	0.222	7.30	2.5	0.000	0.201	0.804
IL-7	Static	0.215	7.30	3.0	0.000	0.207	0.767
IL-6b	Shaking	0.209	7.30	2.5	0.000	0.182	0.736
IL-7b	Shaking	0.208	7.30	2.2	0.000	0.237	0.736
IL-20	Shaking	0.224	7.30	20.0	0.000	0.356	0.675
IL-21	Static	0.169	7.30	25.0	0.000	0.503	0.979
IL-22*	Static	0.204	23.50	274.0	0.000	1.170	-0.153
IL-23	Shaking	0.219	23.50	80.0	0.000	0.193	1.017

* Here σ = slope, ξ = intercept of the square root of time line.

All GEV scaled experiments, excluding IL-22, are shown in **Figure 16**. The result is rather pleasing, and we conclude that our preliminary round of scaling countercurrent imbibition in water-wet rock and with connate water present is a success. We still need to link the coefficients of these scaling curves (τ, σ and ξ) to the petrophysical descriptions of the core samples and the fluids therein.

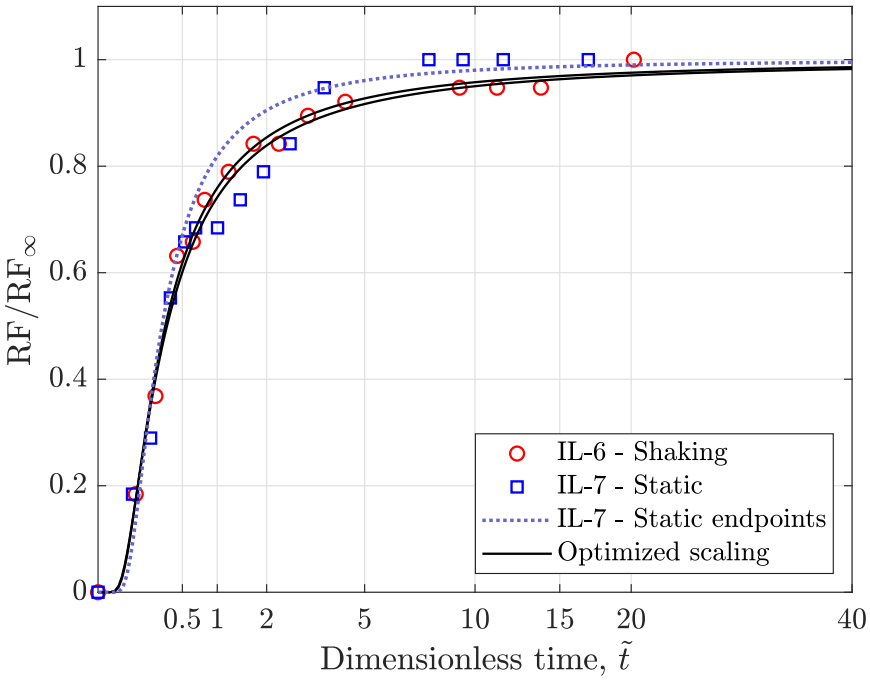

Figure 12: Scaled cumulative recovery versus square root of dimensionless time. Core IL-6, $S_{oi} = 0.69$**, RF**$_\infty = 0.222$**,** $\tau = 2.5$ **hr,** $\sigma = 0.201$**,** $\xi = 0.804$**; core IL-7,** $S_{oi} = 0.70$**, RF**$_\infty = 0.215$**,** $\tau = 3.0$ **hr,** $\sigma = 0.207$**,** $\xi = 0.767$**.**

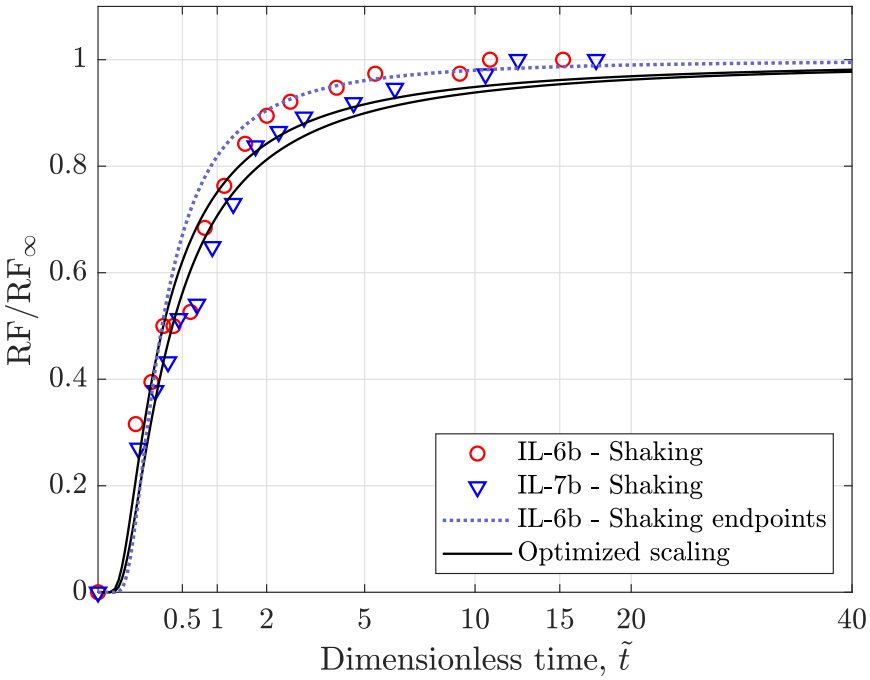

Figure 13: Scaled cumulative recovery versus square root of dimensionless time. Core IL-6b, $S_{oi} = 0.73$**, RF**$_\infty = 0.209$**,** $\tau = 2.5$ **hr,** $\sigma = 0.182$**,** $\xi = 0.736$**; core IL-7b,** $S_{oi} = 0.70$**, RF**$_\infty = 0.208$**,** $\tau = 2.2$ **hr,** $\sigma = 0.237$**,** $\xi = 0.736$**.**

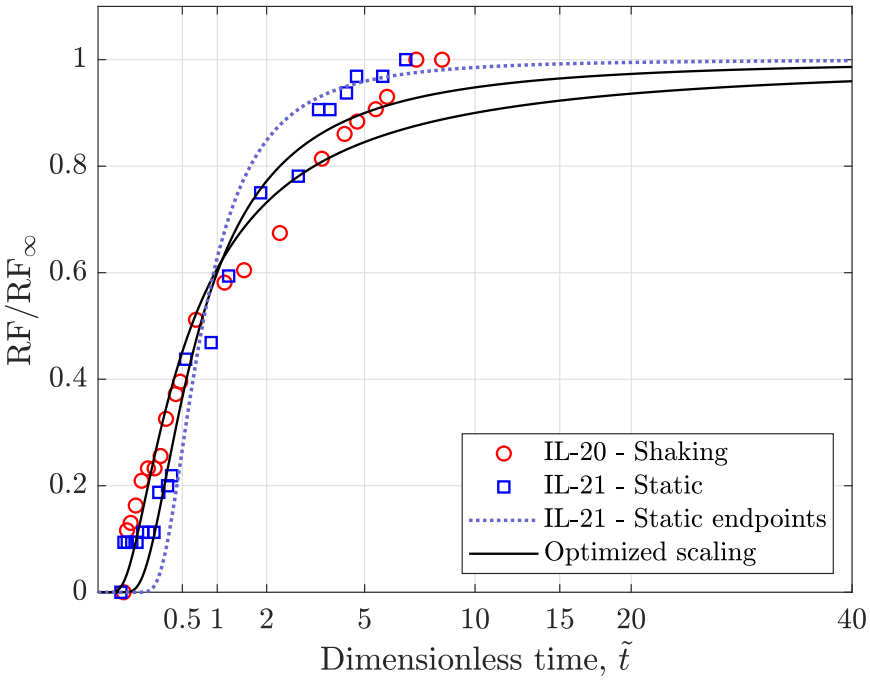

Figure 14: Scaled cumulative recovery versus square root of dimensionless time. Core IL-20, $S_{oi} = 0.73$, **RF**$_\infty = 0.224$, $\tau = 20.0$ **hr,** $\sigma = 0.356$, $\xi = 0.675$**; core IL-21,** $S_{oi} = 0.75$, **RF**$_\infty = 0.169$, $\tau = 25.0$ **hr,** $\sigma = 0.503$, $\xi = 0.979$**.**

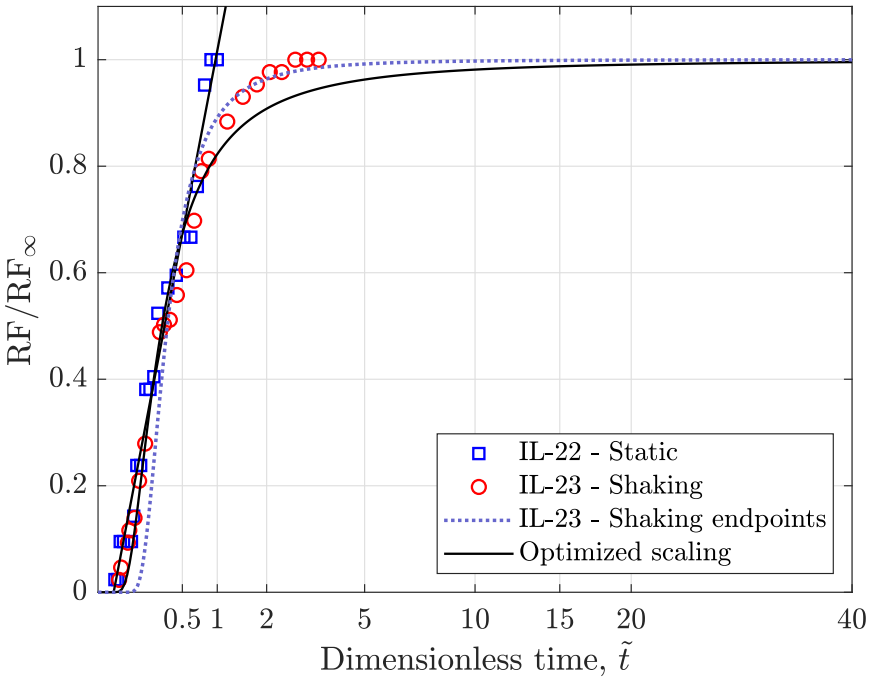

Figure 15: Scaled cumulative recovery versus square root of dimensionless time. Core IL-22, $S_{oi} = 0.81$, **RF**$_\infty = 0.204$, $\tau = 274.0$ **hr,** slope $= 1.170$, intercept $= -0.153$**; core IL-23,** $S_{oi} = 0.72$, **RF**$_\infty = 0.219$, $\tau = 80.0$ **hr,** $\sigma = 0.193$, $\xi = 1.017$**.**

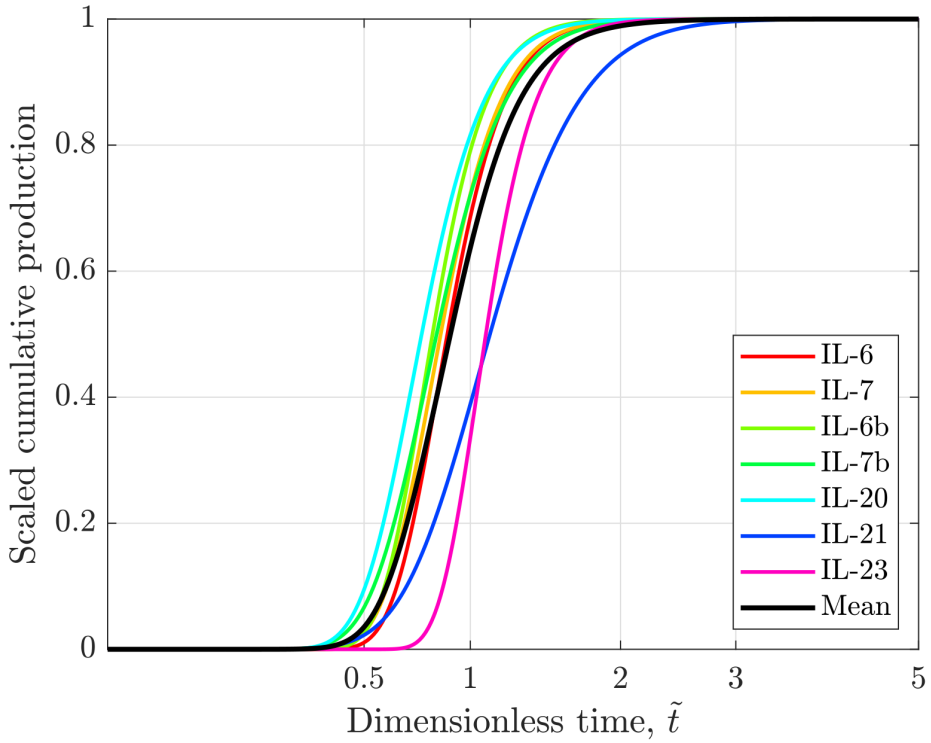

Figure 16: All GEV-scaled cumulative recoveries versus square root of dimensionless time. The "mean" curve is the arithmetic mean of all scaling curves. Experiment IL-22 was scaled with the square root of time line. Note that experiments IL-21 and IL-23 seem to be outliers.

Table 3: Effective water permeability from Amott experiments

ID	Type	α m^2s^{-1}	$d=\sqrt{\tau\alpha}$ m	$d@k_{eff}/k=10^{-5}$ m
IL-6	Shaking	1.759	125.8	0.001
IL-7	Static	3.646	198.0	0.002
IL-6b	Shaking	1.759	125.8	0.001
IL-7b	Shaking	3.646	169.1	0.002
IL-20	Shaking	2.931	606.5	0.006
IL-21	Static	2.401	549.5	0.005
IL-22	Static	3.207	1778.7	0.018
IL-23	Shaking	3.881	1057.3	0.011

The hydraulic diffusivity in water imbibition can be defined (Patzek et al., 2013) as:

$$\alpha = \frac{k_{eff}}{\mu_w c_t \phi} \tag{4}$$

By definition, $\tau = d^2/\alpha$, where d is a reasonable depth of water imbibition in the square root of time flow regime. Assume that this $d = 0.005$ m for our core plug samples. Because the carbonate rock and water are almost incompressible, $c_t \approx \phi c_o$. A typical compressibility of mineral oil is 6.8×10^{-6} psi^{-1} (Busahmin et al., 2017), and brine viscosity at 60 °C is 0.5 mPa s. However in countercurrent flow of brine in pore corner filaments, and with mineral oil that is 15-46 times more viscous and flows in the opposite direction, the brine is subject to viscous drag from oil, and its effective viscosity may be two times higher or more (Patzek and Kristensen, 2001). The last remark pertains especially to the last two experiments in **Table 3**. Either way, from the last column in Table 3, it follows that the effective relative permeability to water is very low, $1 - 5 \times 10^{-5}$. This makes sense, because water flows mostly through corner filaments and the initial resistance to flow at low water saturation is very high.

Conclusions

In this work, we have modified the classical Amott-cell experiment to generate smoother recovery profiles and to obtain more information about dynamics of oil recovery. We have introduced a continuous circular motion of the Amott cell and masked the top and bottom core faces to enforce 1D radial, two-phase flow. The proposed approach allowed us to minimize the holdup effect of the mineral oil droplets on the outer surfaces of Indiana limestone samples and produce smoother experimental production curves. We have then applied Generalized Extreme Value distribution to model the cumulative oil recoveries from all experiments. We have shown that the more accurate experimental production curves of sufficient duration can be scaled with an almost universal GEV curve (Fig. 16). The modified Amott-cell experiment and the developed scaling approach will be implemented in the development of predictive modeling of oil recovery dynamics from mixed-wet carbonates.

Acknowledgements

The authors would like to acknowledge the team of Ali I. Al-Naimi Petroleum Engineering Research Center at King Abdullah University of Science and Technology for the support during the performance of this work. We thank Mahmoud A. Mowafi, Flow assurance drilling technician, and Samuel Fontalvo Guzman, Master student, for sample preparation and execution of the core plug porosity and permeability experiments. Mahmoud A. Mowafi is also thanked for the helpful discussion and literature analysis. We gratefully acknowledge the Saudi Arabian Oil Company for the permission to publish this work.

References

Amott, E. 1959. Observations Relating to the Wettability of Porous Rock. *Published in Petroleum Transactions, AIME, SPE-1167-G* **216**: 156–162.

Ayirala, S., Saleh, S., Enezi, S., and Yousef, A. 2020. Multiscale Aqueous-Ion Interactions at Interfaces for Enhanced Understanding of Controlled-Ionic-Composition-Waterflooding Processes in Carbonates. *SPE Res Eval & Eng* **23** (03): 1118–1132.

Barenblatt, G. and Gilman, A. 1987. A mathematical model of non-equilibrium countercurrent capillary imbibition. *IngPhysJ* **52** (3): 46–461.

Babadagli, T. 2002. Dynamics of Capillary Imbibition When Surfactant, Polymer, and Hot Water Are Used as Aqueous Phase for Oil Recovery. *Journal of Colloid and Interface Science* **246** (1): 203–213.

Barenblatt, G. 1971. Filtration of two nonmixing fluids in a homogeneous porous medium. *Fluid Dynamics* **6** (5): 857–864.

Barenblatt, G. I., Patzek, T. W., and Silin, D. B. 2003. The mathematical model of non-equilibrium effects in water-oil displacement. *SPEJ* **8** (4): 409–416.

Barenblatt, G. I. and Vinnichenko, A. P. 1980. Non-equilibrium seepage of immiscible fluids. *AdvMech* **3** (3): 35–50.

Brady, P. V. and Thyne, G. 2016. Functional Wettability in Carbonate Reservoirs. *Transport in Porous Media* **30** (11): 9217–9225.

Busahmin, B., Maini, B. B., Hasanah, U. B., and Hasan, H. 2017. Influence of Compressibility on Heavy/Foamy Oil Flow. *IOSR Journal of Engineering* **7** (1): 18–27.

Clerke, E., Funk, J., and Shtepani, E. 2013. Spontaneous imbibition of water into oil saturated m_1 bimodal limestone. International Petroleum Technology Conference.

Cobos, J. E., Sandnes, M., Steinsbo, M., Brattekas, B., Sogaard, E. G., and Graue, A. 2021. Evaluation of Wettability Alteration in Heterogeneous Limestone at Microscopic and Macroscopic Levels. *Journal of Petroleum Science and Engineering* **202**: 108534.

Fathi, S. J., Austad, T., and Strand, S. 2010. "Smart Water" as a Wettability Modifier in Chalk: The Effect of Salinity and Ionic Composition. *Energy Fuels* **24** (4): 2514–2519.

Ghedan, S. G., Canbaz, C. H., and Mtawaa, B. 2009. Effect of shape factor, IFT and amott method derived wettability on the imbibition process. International Petroleum Technology Conference.

Graue, A., Viksund, B. G., Eilertsen, T., and Moe, R. 1999. Systematic Wettability Alteration by Aging Sandstone and Carbonate Rock in Crude Oil. *Journal of Petroleum Science and Engineering* **24** (2-4): 85–97.

Gumbel, E. J. 1958. *Statistics of Extremes*. Columbia University Press, New York.

Kashchiev, D. and Firoozabadi, A. 2002. Analytical solutions for 1-d countercurrent imbibition in water-wet media. SPE.

Lenormand, R. 1986. Pattern growth and fluid displacements through porous media. *Physica A* **140**: 114–123.

Lenormand, R. 1989. Flow through porous media: Limits of fractal patterns. *Proc. R. Soc. Lond. A* **423**: 159–168.

Lenormand, R. 1990. Liquids in porous media. *Physics of Condensed Matter* **2** (SA): 79–88.

Lenormand, R. and Zarcone, C. 1989. Capillary fingering: Percolation and capillary fingering. *Transport in Porous Media* **4**: 599–612.

Liu, J., Sheng, J. J., and Tu, J. 2020. Effect of Spontaneous Emulsification on Oil Recovery in Tight Oil-Wet Reservoirs. *Journal of Petroleum Science and Engineering* **279**: 118456.

Moore, T. and Slobod, R. 1955. Displacement of oil by water-effect of wettability, rate, and viscosity on recovery. SPE.

Morrow, N., Ma, S., Zhou, X., and Zhang, X. 1999. Characterization of Wettability From Spontaneous Imbibition Measurements. *Journal of Canadian Petroleum Technology* **38** (13).

Morrow, N. R. and Mason, G. 2001. Recovery of Oil by Spontaneous Imbibition. *Current Opinion in Colloid & Interface Science* **6**: 321–337.

Muskat, M. 1937. *The Flow of Homogeneous Fluids Through Porous Media*. McGraw-Hill Book Company, Inc., New York.

Patzek, T. W. 2001. Verification of a complete pore network model of drainage and imbibition. *SPEJ* **6** (2): 144–156.

Patzek, T. W. and Kristensen, J. 2001. Shape factor and hydraulic conductance in noncircular capillaries: II. Two-phase creeping flow. *J. Colloid and Interface Sci.* **296**: 305–317.

Patzek, T. W., Male, F., and Marder, M. 2013. Gas production in the Barnett shale obeys a simple scaling theory. *Proceedings of the National Academy of Sciences* **110** (49): 19731–19736.

Rapoport, L. A. and Leas, W. J. 1953. Properties of linear waterfloods. *AIME* **216**: 139–148.

Richards, L. A. 1928. The usefulness of capillary potential to soil moisture and plant investigations. *J. Agricultural Research* **37**: 719–742.

Richards, L. A. 1931. Capillary conduction of liquids through porous medium. *Physics* **1**: 318–333.

Roof, J. 1970. Snap-Off of Oil Droplets in Water-Wet Pores. *SPE J., SPE-2504-PA* **10** (01): 85–90.

Saad, A. M., Yutkin, M. P., Radke, C. J., and Patzek, T. W. 2022. Pore-Scale Spontaneous Imbibition at High Advancing Contact Angles in Mixed-Wet Media: Theory and Experentim. *Energy & Fuels. Accepted* .

Silin, D. B. and Patzek, T. W. 2004. On the Barenblatt model of non-equilibrium imbibition. *TPM* **54**: 297–322.

Tang, G.-Q. and Firoozabadi, A. 2001. Effect of Pressure Gradient and Initial Water Saturation on Water Injection in Water-Wet and Mixed-Wet Fractured Porous Media. *SPE Res Eval & Eng, SPE-74711-PA* **4** (06): 516–524.

Yousef, A. A., Liu, J., Blanchard, G., Al-Saleh, S., Al-Zahrani, T., Al-Zahrani, R., Al-Tammar, H., and Al-Mulhim, N. 2012. SPE.

Yutkin, M., Radke, C., and Patzek, T. 2021. Chemical Compositions in Salinity Waterflooding of Carbonate Reservoirs: Theory. *Transport in Porous Media* **136**: 411–429.

Yutkin, M. P., Radke, C. J., and Patzek, T. W. 2022. Chemical compositions in modified salinity waterflooding of calcium carbonate reservoirs: Experiment. *Transport in Porous Media* .

Zhang, P., Tweheyo, M. T., and Austad, T. 2006. Wettability Alteration and Improved Oil Recovery in Chalk: The Effect of Calcium in the Presence of Sulfate. *Energy Fuels* **20** (5): 2056–2062.

Zhou, D., Jia, L., Kamath, J., and Kovscek, A. R. 2001. An investigation of counter-current imbibition processes in diatomite. SPE 68837. Bakersfield, CA. 2001 SPE Western Reginal Meeting.

Zhou, X., Morrow, N., and Ma, S. 2000. Interrelationship of Wettability, Initial Water Saturation, Aging Time, and Oil Recovery by Spontaneous Imbibition and Waterflooding. *SPE Journal* **5** (2): 199–207.